

ANTHRAQUINONE DERIVATIVES BEARING THIADIAZOL MOIETY, DESIGN, SYNTHESIS, CHARACTERIZATION, AND CYTOTOXIC EVALUATION

MOHAMMED ISMAIL MOHAMMED^{1*}, MOHAMMED HASSAN MOHAMMED²

¹Ministry of Health, Karbala, Iraq, Al Naqeeb Street, 2567, Iraq. ²Department of Pharmaceutical Chemistry, Pharmacy College, Baghdad University, Baghdad, Iraq.

*Corresponding author: Mohammed Ismail Mohammed; Email: mohammed.ismail2200m@copharm.uobaghdad.edu.iq

Received: 08 July 2025, Revised and Accepted: 20 August 2025

ABSTRACT

Objectives: The primary goals were to study biological activity *in vivo*, 3-(4,5-dimethylthiazol-2-yl)-2,5-diphenyltetrazolium bromide (MTT) cell viability assay, the synthesis of new anthraquinone derivatives MI(6-9) bearing heterocyclic scaffolds(1,3,4-thiadiazole), and molecular docking studies.

Methods: Molecular docking studies (using Ligand Designer from Glide [Schrodinger LLC]) for the proposed compounds against Vegfr2 and topoisomerase II receptors with sunitinib and doxorubicin as references, respectively. The synthesis of new anthraquinone derivatives MI(6-9) bearing heterocyclic scaffolds(1,3,4-thiadiazole), characterized through melting point, TLC, and spectral data acquisition (infrared [IR], attenuated total reflectance-Fourier transform IR, nuclear magnetic resonance), and evaluated *in vivo* using an MTT cytotoxicity assay with sunitinib and doxorubicin as a standard.

Results: The docking score of compound MI8 is (-7.403), which is higher than sunitinib (-7.086), while MI6 and MI7 are slightly lower than it. The docking scores of compounds MI8 (-5.194), MI6 (-4.887), and MI9 (-4.843) are higher than that of doxorubicin (-4.761). The results of the cytotoxicity study showed that the compound MI8 exhibited the most potent inhibitory activity, comparable to sunitinib and doxorubicin, since its inhibitory concentration (IC₅₀) is 3.00 µg/mL, while sunitinib has 6.89 µg/mL and doxorubicin has 2.89 µg/mL in the breast cancer cell line, while in the lung cancer cell line, the compound MI8 has an IC₅₀ of 4.10 µg/mL, but sunitinib has 3.00 µg/mL and doxorubicin has 2.83 µg/mL. GraphPad Prism 8.5 was used for data analysis and graphing software.

Conclusion: The molecules (MI6–MI9) that were designed were successfully synthesized, and MI8 demonstrated superior cell inhibition activity, which indicated a high potential for antiproliferative function.

Keywords: 1,3,4-Thiadiazole, Anthraquinone, Anticancer, Cytotoxic Evaluation, Heterocyclic compounds.

© 2025 The Authors. Published by Innovare Academic Sciences Pvt Ltd. This is an open access article under the CC BY license (<http://creativecommons.org/licenses/by/4.0/>) DOI: <http://dx.doi.org/10.22159/ajpcr.2025v18i9.56543>. Journal homepage: <https://innovareacademics.in/journals/index.php/ajpcr>

INTRODUCTION

Cancer ranks as the second leading cause of mortality globally, claiming over 8 million lives annually; its incidence is projected to rise by over 50% in the forthcoming decades [1]. Cancer encompasses a diverse array of types, each characterized by distinct etiologies, clinical manifestations, and associated risk factors. The importance of early detection and preventive measures cannot be overstated, as they are pivotal in managing and potentially mitigating the progression of all forms of cancer. Cancer is caused by mutations in a cell's DNA. Mutations can arise due to a combination of factors, including genetic predisposition, exposure to environmental toxins, adoption of unhealthy lifestyle practices, and the influence of viral infections [2-4]. Anticancer medications, also referred to as antineoplastic drugs, are pharmaceuticals designed to combat cancer or other malignant conditions. These drugs are categorized into various types, such as hormones, alkylating agents, antimetabolites, and natural compounds [5].

The anthraquinone structure exhibits a rigid configuration, characterized by a planar, aromatic anthracene system composed of three fused rings and featuring keto functional groups at the 9th and 10th positions. This planar core can intercalate within the DNA double helix of cancer cells to enable a specialized redox cycle producing anions of superoxide radicals (O₂⁻) [6,7] (Fig.1).

Anthraquinones demonstrate significant anticancer properties, which have been the subject of extensive investigation since their identification. Over time, medicinal chemists have creatively explored

numerous structural modifications, paving the way for the development and synthesis of a wide array of anthraquinone derivatives. These innovative compounds have demonstrated a remarkable range of biological activities, highlighting their diverse potential in various biomedical applications. Conventionally, these compounds are thought to combat cancer by inducing apoptosis, causing cell cycle arrest, and eliciting DNA damage. Recent research suggests that new anthraquinone compounds could play a significant role in halting cancer progression. These compounds appear to act through various mechanisms, such as inducing paraptosis, promoting autophagy, enhancing radiosensitivity, tackling chemoresistance, and leveraging other advanced therapeutic pathways [6,8].

There are several studies that have made hybrids between anthraquinone and heterocyclic compounds in order to increase effectiveness and reduce side effects. These studies have also proven that these hybrids act as multitarget compounds and multiply the cytotoxic activity [9,10]

Heterocyclic substances are defined by their presence of a fully conjugated system of double bonds and the incorporation of one or more heteroatoms, such as oxygen, sulfur, or nitrogen, into their molecular framework alongside carbon and hydrogen [11,12]. The field of heterocyclic chemistry, a dynamic and rapidly evolving branch of organic chemistry, plays a pivotal role in modern synthetic methodologies. By 1998, heterocyclic compounds accounted for nearly 60% of all synthetic processes, underscoring their significant contribution to the advancement of chemical synthesis [13].

Recent publications on novel heterocyclic compounds span diverse disciplines, including biology, materials science, and medicine. A variety of compounds containing five-membered heterocyclic rings demonstrates exceptional chemical properties and serves numerous biological functions [14].

Research indicates that 1,3,4-thiadiazole derivatives stand out as one of the most promising groups of compounds, showcasing significant potential for therapeutic applications [15]. Research indicates that compounds based on the 1,3,4-thiadiazole group exhibit a wide array of therapeutic effects, including antibacterial, anti-inflammatory, antitubercular, antipsychotic, antifungal, analgesic, anticonvulsant, antidepressant, and anti-leishmanial activities. In addition, extensive studies have provided substantial evidence of their potent anti-cancer capabilities [16,17]. The aromatic properties of the ring significantly influence a wide range of biological functions demonstrated by derivatives of 1,3,4-thiadiazole. This characteristic improves the stability of the five-membered ring structure *in vivo* while significantly reducing toxicity in larger animals, including humans [18].

Globally, breast cancer ranks as the second most prevalent cancer, with an estimated 2.11 million new cases and nearly 626,000 fatalities attributed to the disease in 2018. Breast cancer is a clinically and biologically heterogeneous disease characterized by multiple histotypes and molecular subtypes, each with distinct etiologies, risk factor profiles, treatment responses, and prognoses [19].

Lung cancer is a prevalent and highly aggressive malignancy, with approximately 2.2,000,000 new diagnoses and 1.8 million fatalities globally in 2020. It continues to be the primary cause of cancer-related mortality in men worldwide and is the 2nd most lethal cancer in women, after breast cancer [20]. Men have double the likelihood of being diagnosed with lung cancer, primarily due to disparities in tobacco use; however, Women may experience increased susceptibility because of a higher prevalence of epidermal growth factor receptor mutations and the influence of estrogen. A family history significantly increases the likelihood, raising the risk by approximately 1.7 times, particularly among first-degree relatives. Smoking remains the leading preventable cause of death worldwide, accounting for nearly 90% of lung cancer cases [21].

Protein kinases (PK) play a crucial role in virtually all cellular activities. They regulate metabolic pathways, transcription processes, cell division, movement, programmed cell death, immune system responses, and the functioning of the nervous system [22]. Within the human genome, PK genes form the third-largest superfamily, comprising around 2% of its total composition. These genes encode vital regulatory enzymes responsible for modulating a diverse array of cellular activities through the phosphorylation of their protein targets. However, the transcriptional mechanisms governing the expression of PK genes remain intricate and not yet completely elucidated [23].

Unfortunately, I don't have the time to do these assays and don't have these acknowledgments in my area; otherwise, I would send my compounds to another country to do it. I'm sorry for that.

*Clarify why Vegfr2 and topoisomerase II were chosen as targets. Are these pathways relevant to the tested cell lines (MDA-MB-231, A549)?

First, I chose topoisomerase II because my compounds are synthesized from an anthraquinone core, just like Doxorubicin, so we think they will resemble the activity of Doxorubicin (which targets topoisomerase II). Then we do target prediction for the compounds and notice that they have a good activity against protein kinases. So, we chose them and did a molecular docking against them.

Yes, both Vegfr2 and topoisomerase II play significant roles in the context of lung and breast cancer, and they are often involved in targeted therapies or cancer treatment strategies.

*Specify purity of compounds (HPLC/LC-MS data) and reproducibility of synthesis (yields, reaction conditions).

We use a column chromatography technique for the purification of the compounds. The stationary phase used is silica (60–120 mesh). Using the dry method, silica was packed into a column and neutralized using triethylamine with hexane as eluent before the application of the sample. Ethyl acetate, n-hexane in different ratios were used as a mobile phase. All fractions were collected and monitored using TLC to verify the presence of the wanted product, and do not use (HPLC/LC-MS data) because it is unavailable.

*Clarify solvent systems for TLC (e.g., hexane: Ethyl acetate ratios in System A/B) and melting point ranges (are they sharp?)

Compound code	Chemical formula	M. wt. (g/mol)	Physical property	Melting point °C	Solvent system used
1	C ₂ H ₃ N ₃ S ₂	133.19	White powder	239–241°C	A
2f	C ₉ H ₈ N ₄ O ₂ S ₂	268.31	Yellow crystals	174–177°C	B
2g	C ₉ H ₈ N ₄ O ₂ S ₂	268.31	Yellowish green crystals	184–1188°C	B
2h	C ₁₀ H ₁₁ N ₃ OS ₂	253.34	Off-white powder	169–172°C	A
2i	C ₁₀ H ₁₁ N ₃ OS ₂	253.34	Pale yellow powder	185–187°C	A
MI6	C ₂₄ H ₁₄ N ₄ O ₅ S ₂	502.52	Pale yellow powder	187–189°C	A
MI7	C ₂₄ H ₁₄ N ₄ O ₅ S ₂	502.52	Yellow crystalline powder	222–226°C	A
MI8	C ₂₅ H ₁₇ N ₃ O ₄ S ₂	487.55	Off white powder	213–216°C	A
MI9	C ₂₅ H ₁₇ N ₃ O ₄ S ₂	487.55	Yellow powder	237–239°C	A

*Justify the use of Glide (Schrödinger) and parameters (e.g., grid box size, ligand flexibility). Include RMSD values for docking validation (currently mentioned but not interpreted).

The molecular docking was carried out using Glide, an advanced software program created by Schrödinger (version 2023), modeling suite version 13.0135. The binding sites used in the analysis were provided by the ligand that was co-crystallized with the crystal protein (PDB codes: 2OH4 and 5GWK). The protein preparation workflow built into the Maestro software was then used to prepare the proteins. This included preprocessing the protein to determine bond order, replacing hydrogen, filling in missing loops with Prime, generating het states (using Epike) at pH 7.4, and minimizing using force field OPLS_2005.

Water molecules that were more than three Å away from ligands were eliminated. The co-crystallized ligand served as the primary reference point to create the boundary box for the protein grid. The size of the boundary box that was utilized was 12 Å*12 Å*12. Å). The Maestro program's 2D Sketcher was used to sketch the designed ligands. Using force field OPLS_2005, LigPrep in the Maestro suite optimized ligand structures to produce potential states at target pH 7, desalt, and produce tautomers. The prepared ligands were written out in no more than five poses per ligand.

The RMSD value is 1.9072 when docking the compounds with the Vegfr2 binding site, while the RMSD value is 0.2394 when docking the compounds with the topoisomerase II binding site; they both are good as long as they are below 2.

METHODS

Materials

Chemicals	Company	Country
Acetone	Thomas baker	India
Carbon disulfide	Sigma-Aldrich	UAS
Anthraquinone 2-carboxylic acid	Fluorockem	UK
Diethyl ether	Thomas baker	India
Doxorubicin	MACKLIN	China
Ethanol	haymankimia	UK
Ethyl acetate	haymankimia	UK
Magnesium sulphate (MgSO ₄)	Alphachem.	India
3-methoxybenzyl chloride	MACKLIN	China
4-methoxybenzyl chloride	MACKLIN	China
N-hexane	LobaCheme	India
2-nitrobenzyl chloride	MACKLIN	China
4-nitrobenzyl chloride	MACKLIN	China
Petroleum ether	Sigma-Aldrich	UAS
Potassium carbonate	Cholera toxin Sigma	Germany
Sodium bicarbonate	VWR	USA
Sunitinib	MACKLIN	China
Thionyl chloride	Sigma-Aldrich	UAS
Thiosemicarbazide	Sigma-Aldrich	UAS
Trimethylamine 99.5%	LobaCheme	India
Tetrahydrofuran	LobaCheme	Germany

Instrumentation

Equipment	Company	Origin
ART-FT-IR spectrophotometer	Shimadzu	Japan
Electrical melting point apparatus (SMP30)	Stuart	Germany
Electric oven	Lab. Tech	South Korea
Hot plate and magnetic stirrer	Stuart	Germany
¹ H-NMR	Bruker	Korea
Rotary evaporator	BUCHI	Germany
Sartorius balance	Weke-GMBH	Germany
Thin-layer chromatography	Merck	Germany
Ultraviolet lamp	Allen	England

Procedu0re

Synthesis of the intermediate 1,2-amino-5-mercapto-1,3,4-thiadiazole

Within a 250 mL round-bottom flask, 4 g of thiosemicarbazide (0.043 moles) was dissolved in 30 mL of absolute ethanol. Subsequently, 9.5 g of carbon disulfide (0.125 moles) and 2.23 g of anhydrous sodium carbonate (0.021 moles) were introduced into the mixture under continuous stirring. After 5 h of reflux (80°C), the reaction mixture was allowed to cool to room temperature before being filtered. After the filtrate was vacuum-evaporated, cold distilled water, measuring 90 mm, was added, and then concentrated HCl was gradually added to acidify the mixture until a white-yellowish precipitate formed. After filtering and washing with distilled water, this precipitate was recrystallized with hot distilled water [24,25].

Intermediate 1 is obtained as a white powder with an 80% yield and a melting point of 239–241°C. The FT-IR (ATR; ν , cm⁻¹) spectrum displays characteristic absorption bands at 3325 and 3244 for NH₂ stretching of the primary amine, and at 1604 for C=N stretching, indicating the presence of an imine bond.

Synthesis of intermediate 2f-2i

To synthesize compounds 2f–2i, initiate the process by dissolving 0.70 g (equivalent to 5 mmol) of compound 1 into 25 mm of ethanol within a 250-mm round-bottom flask. Following this step, introduce 0.75 mm (5 mmol) of triethylamine into the solution. Ensure the mixture is stirred continuously for a duration of 10 min. Subsequently, add 5 mmol of each derivative slowly, using a dropwise technique, to maintain controlled reaction conditions. The derivatives include 0.85 g of 2-nitrobenzyl chloride, 0.85 g of 4-nitrobenzyl chloride, 0.78 g of 3-methoxybenzyl chloride, and 0.78 g of 4-methoxybenzyl chloride. Maintain steady stirring throughout the addition and allow the mixture

to stir overnight (at room temperature) to ensure the reaction proceeds efficiently. Once the reaction is complete, collect the resulting solid precipitate by filtration. Wash the solid thoroughly several times with cold water to remove any impurities or residue. Finally, dry the purified product to obtain the expected compounds, labeled as 2f–2i, ready for further analysis or use [26–28].

5-((2-nitrobenzyl) thiol)-1,3,4-thiadiazole-2-amine (2f)

A yellow crystalline solid was obtained with a yield of 85% and a melting point ranging between 174°C and 177°C. The characterization through FT-IR spectroscopy using ATR mode (ν , cm⁻¹) revealed distinct absorption bands: 3278, corresponding to NH stretching of the primary amine; 3074, indicative of aromatic C-H stretching; 2951, associated with aliphatic C-H stretching; 1635, representing C=N stretching attributable to the imine functional group; and 1504, signifying C=C stretching within the aromatic ring system.

5-((4-nitrobenzyl) thiol)-1,3,4-thiadiazole-2-amine (2g)

Yellowish-green crystals were obtained, boasting a 75% yield with a melting point range from 184 to 188°C. The FT-IR analysis conducted using ATR revealed several distinct peaks: at 3275 cm⁻¹, there was the NH stretching indicative of a primary amine; the aromatic ring showed C-H stretching at 3093 cm⁻¹. Moreover, the aliphatic C-H stretching appeared at 2954 cm⁻¹. In addition, the imine bond was evident through C=N stretching at 1631 cm⁻¹, and the aromatic ring was further characterized by C=C stretching at 1523 cm⁻¹. These detailed analyses provide valuable insights into the molecular structure of the crystals.

5-((3-methoxybenzyl) thiol)-1,3,4-thiadiazole-2-amine (2h)

An off-white powder was obtained with an 80% yield. The measured melting point ranged between 169–172°C. FT-IR (ATR) analysis revealed notable absorption bands (ν , cm⁻¹) as follows: 3305 and 3259, corresponding to the NH stretching vibrations of a primary amine, are observed at 3082, corresponding to C-H stretching in the aromatic ring. In addition, the signal at 2966 represents aliphatic C-H stretching, while the peak at 1631 is indicative of C=N stretching associated with the imine bond. Finally, the absorption at 1492 is linked to the stretching of C=C within the aromatic ring.

5-([4-methoxybenzyl] thiol)-1,3,4-thiadiazole-2-amine (2i)

A pale-yellow powdered compound was synthesized, achieving a yield of 70%, with a melting point range determined to be 185–187°C. Fourier-transform infrared (FT-IR) spectroscopy conducted using attenuated total reflectance (ATR) mode provided key spectral data (ν , cm⁻¹), identifying significant absorption bands. A peak at 3315 cm⁻¹ was attributed to the NH stretching vibration of a primary amine group, while another at 3088 cm⁻¹ corresponded to aromatic C-H stretching vibrations. In addition, a band at 2931 cm⁻¹ was linked to aliphatic C-H stretching. The absorption observed at 1629 cm⁻¹ indicated C=N stretching, characteristic of an imine bond, and the peak at 1512 cm⁻¹ was associated with C=C stretching vibrations within the aromatic ring structure.

Synthesis of anthraquinone derivatives (MI6–MI9)

In a 100 mL round-bottom flask, 0.5 g (2 mmol) of anthraquinone-2-carboxylic acid was evenly dispersed in 10 mL of anhydrous chloroform, utilizing anhydrous magnesium sulfate to ensure the reaction medium remained moisture-free. The reaction mixture was subsequently cooled by immersion in an ice bath for a duration of 10 min to maintain a low-temperature environment conducive (0°C) to the reaction process. At this time, SOCl₂ (0.7 mL, 9.8 mmol) was slowly added with continuous stirring to ensure proper mixing. A hot air stream was used to evaporate the reaction mixture to dryness after it had refluxed for 3 h. The mixture was then redissolved in 3 mm of dry chloroform and evaporated twice more. The oil was dissolved in 1 mm of dry chloroform so that it could be used fresh in the following step.

For each compound (2f, 2g, 2h, and 2i), amounting to a total of 1 mmol (specifically, 0.27 g of 2f, 0.27 g of 2g, 0.25 g of 2h, and 0.5 g of 2i), the

substance was individually dissolved in 25 mL of dichloromethane inside a 250 mL flask placed in icy bath. Subsequently, TEA (0.3 mL, corresponding to 2 mmol) was introduced dropwise over the course of 2 min. The reaction mixture was then stirred continuously at 0°C for 2 h. Meanwhile, a solution of dry chloroform (1 mL) mixed with an equimolar amount of anthraquinone acid chloride was prepared. This solution was carefully gradually introduced to the reaction mixture, and stirred at the same temperature for an additional 2 h. Afterward, the setup was left undisturbed overnight at room temperature (25°C). Following the completion of the reaction, the solvent was removed under vacuum. The residue obtained was dissolved in 30 mL of ethyl acetate and filtered to separate any insoluble impurities. The filtrate obtained was transferred into a separatory funnel and underwent a series of successive washes: First with 10 mL of hydrochloric acid (HCl), then with 10 mL of distilled water, followed by 10 mL of 5% sodium bicarbonate solution, and finally with another 10 mL of distilled water. The organic layer was meticulously separated and dried using anhydrous magnesium sulfate to remove any residual moisture. Afterward, it underwent filtration to ensure purity. The filtrate was then subjected to evaporation under reduced pressure, resulting in an oily residue, which represented the MI6-MI9 compounds [29,30].

n-(5-((2-nitrobenzyl)thiol)-1,3,4-thiadiazole-2-yl)-9,10-dioxo-9,10-dihydroanthracen-2-carboxamid (MI6)

A pale-yellow powder was synthesized with an isolated yield of 80% and a melting point range of 186–189°C. Fourier Transform Infrared (FT-IR) spectroscopy employing Attenuated Total Reflectance (ATR) analysis (in cm^{-1}) identified characteristic absorption bands corresponding to functional groups within the compound: 3170 (secondary amine NH stretching), 3039 (aromatic C–H stretching), 2953 (aliphatic C–H stretching), 1676 (C=O stretching for a ketone), and 1646 (C=O stretching associated with an amide functionality). The proton nuclear magnetic resonance ($^1\text{H-NMR}$) spectrum, recorded at 400 MHz in dimethyl sulfoxide (DMSO), exhibited distinct signals at δ 4.63 (a singlet integrating for 2H, attributed to CH_2), δ 7.53–8.54 (a multiplet integrating for 11H, consistent with protons in an aromatic framework), and δ 12.22 (a singlet corresponding to 1H, indicative of an NH moiety).

n-(5-((4-nitrobenzyl)thiol)-1,3,4-thiadiazole-2-yl)-9,10-dioxo-9,10-dihydroanthracen-2-carboxamid (MI7)

A yellow crystalline powder with a melting point in the range of 222–226°C and a 65% yield was obtained. FT-IR (ATR, ν , cm^{-1}): 3165 corresponds to the NH stretching of a secondary amine, 3066 indicates aromatic C–H stretching, 2958 indicates aliphatic C–H stretching, 1673 corresponds to the C=O stretch of a ketone, and 1654 corresponds to the C=O stretch of an amide. The chemical shifts of the $^1\text{H-NMR}$ (400 MHz, DMSO) were as follows: δ 4.54 (singlet, 2H from CH_2), 7.62–8.55 (multiplet, 11H from aromatic protons), and 12.28 (singlet, 1H from NH).

n-(5-((3-methoxybenzyl)thiol)-1,3,4-thiadiazole-2-yl)-9,10-dioxo-9,10-dihydroanthracen-2-carboxamid (MI8)

A pale off-white powder was obtained with a yield of 55% and a melting point range of 213–216°C. FT-IR analysis (ATR; ν , cm^{-1}) reveals characteristic absorption bands at 3175, indicating NH stretching of a secondary amine; 3037, corresponding to aromatic C–H stretching; 2950, associated with aliphatic C–H stretching; 1674, representing the C=O stretch of a ketone; and 1652, attributed to the C=O stretch of an amide. The $^1\text{H-NMR}$ spectrum (400 MHz, DMSO) shows resonances at δ 3.74 (a singlet corresponding to 3H of OCH_3), δ 4.69 (a singlet for 2H of CH_2), δ 6.82–8.58 (a multiplet accounting for 11 aromatic protons), and δ 12.13 (a singlet corresponding to 1H of NH).

n-(5-((4-methoxybenzyl)thiol)-1,3,4-thiadiazole-2-yl)-9,10-dioxo-9,10-dihydroanthracen-2-carboxamid (MI9)

The compound was synthesized as a yellow powder, achieving a yield of 60% with a melting point in the range of 237 to 239°C. FT-

IR spectroscopy analysis using Attenuated Total Reflectance (ATR) revealed key absorptions at wavenumbers of 3163 cm^{-1} , indicating NH stretching of the secondary amine; 3058 cm^{-1} , corresponding to C–H stretching of the aromatic ring; 2924 cm^{-1} , denoting aliphatic C–H stretching; 1676 cm^{-1} , associated with C=O stretching of the ketone; and 1653 cm^{-1} , related to C=O stretching of the amide. Proton nuclear magnetic resonance ($^1\text{H-NMR}$) spectroscopy, conducted at 400 MHz in DMSO solvent, exhibited signals at chemical shifts of δ 3.63 ppm as a singlet (3H, corresponding to the methoxy group OCH_3), δ 4.27 ppm as a singlet (2H, from methylene group CH_2), δ 6.86–8.57 ppm as a multiplet (11H, corresponding to aromatic protons), and δ 12.38 ppm as a singlet (1H, attributed to the NH group).

Molecular docking

Finding molecular targets requires careful evaluation of the functional potential of the recently produced compounds MI6–MI9 and thorough ligand comparison. The pharmacophoric characteristics that support effective binding to important amino acid residues within the target site are aimed to be found by this study. Using Protein Data Bank (<https://www.rcsb.org/>) data helped to guide the careful choice of a binding site. The compounds were thoroughly tested across several binding sites to evaluate their interactions; the findings gave important new perspectives on the identification of appropriate proteins for next docking studies.

Following the identification of a particular protein as the target site, a sequence of rigorous techniques was followed to assess the molecular binding interactions of the investigated compounds inside the binding pocket of the receptor. Glide, a futuristic tool created by Schrödinger (version 2023), was used for molecular docking. Binding sites for the analysis were obtained from ligand co-crystallized in tandem with a crystal protein (PDB codes: 2OH4 and 5GWK). Water molecules in the protein-ligand complexes were first eliminated, then crystallographic defects or unoccupied valence atoms were fixed using the clean protein functions, utility tools, and protein reporting tools of the program [31,32].

The RMSD value is 1.9072 were docking the compounds with the Vegfr2 binding site, while the RMSD value is 0.2394 when docking the compounds with the topoisomerase II binding site.

Cell lines and culturing techniques

Acquired from the National Cell Bank of Iran, affiliated with the Pasteur Institute of Iran, were the A549 human lung cancer cell line and the MDA-MB-231 human breast cancer cell line. Using RPMI-1640 media (Gibco), the cells were cultivated in supplemented with 10% foetal bovine serum (FBS, Gibco) and a mix of antibiotics comprising 100 $\mu\text{g/mL}$ streptomycin and 100 U/mL penicillin. Maintaining a temperature of 37°C in a humidified environment with 5% CO_2 , cultivation conditions were to guarantee their viability and steady development. Routine cell passaging was carried out with a trypsin-EDTA solution (Gibco) and phosphate-buffered saline (PBS).

The MTT assay

Cell growth and viability were assessed using the MTT assay (3-[4,5-dimethylthiazol-2-yl]-2,5-diphenyltetrazolium bromide) (Sigma-Aldrich). Briefly, cells were treated with trypsin for digestion, harvested, and adjusted to a density of 1.4×10^4 cells per well. They were then plated in 96-well plates containing 200 μL of fresh medium per well and incubated for 24 h. After a monolayer was established, cells were exposed to various concentrations (50–3.125 $\mu\text{g/mL}$) of each compound dissolved in DMSO for 72 h at 37°C under 5% CO_2 conditions. At the end of the 72-h treatment period, the supernatant was carefully removed from the plate while leaving the cell monolayer intact. Subsequently, 200 μL of MTT solution (0.5 mg/ml in phosphate-buffered saline [PBS]) was added to each well, and the plate was incubated for an additional 4 h at 37°C. Following this incubation, the MTT solution was discarded, and 100 μL of dimethyl sulfoxide (DMSO) was introduced to each well. The plate was then placed on a shaker

at 37°C to ensure complete dissolution of the formazan crystals. Cell viability was assessed by measuring absorbance at 570 nm using an ELISA reader (Model Wave XS2, BioTek, USA). The half-maximal IC₅₀ values for the compounds were calculated from dose-response curves, reflecting their respective impacts on inducing cell death.

RESULTS AND DISCUSSION

In general, we tried to benefit from previous studies (especially the following studies) in the manufacturing of amide derivatives of anthraquinone and linking them with the thiadiazol group to achieve compounds with stronger activity.

Ali, Lee *et al.* developed two novel compounds tested against 60 and 39 cancer cell lines. They created powerful anthraquinone-derived compounds with reduced adverse effects by attacking the anthraquinone core with a thiadiazolering [33]. Malik *et al.* synthesized amide anthraquinone derivatives to target cancer cells, showing potency in HCT116 cells and causing tumor cell apoptosis [34].

Results of molecular docking analysis

The molecular docking analysis highlighted the binding energies between ligands and receptors, as demonstrated by the differing G-Scores [35]. Compounds MI8 exhibit a higher docking score compared to sunitinib, whereas MI6 and MI7 show slightly lower scores, as presented in Table 1. In addition, the docking scores of MI8, MI6, and MI5 surpass that of doxorubicin, as illustrated in Table 2.

The docking score for sunitinib was noted to be (-7.086) kcal/mole, indicating a strong binding affinity. This strong interaction is corroborated by crucial hydrogen bond formations between the carbonyl group and the Cys917. Furthermore, Pi-pi stacking of PHE1045 with the pyrrole ring.

These particular interactions are crucial for stabilizing the ligand within the enzyme's active site, thereby augmenting its inhibitory effect.

In respect to compound MI8, which docked with Vegfr2, exhibited a docking score of (-7.403) kcal/mol, higher than that of sunitinib. The binding of this compound involved a hydrogen bond between the nitrogen atom of the thiadiazol ring and CYS917, and hydrogen bonds between the carbonyl group and ASN921, indicating strong binding forces (Fig.2).

Concerning doxorubicin, which has a docking score of (-4.761), its binding affinity is corroborated by crucial hydrogen bond formations of VAL160, TRP108, and LEU103 with the hydroxyl groups of doxorubicin.

Table 1: The docking scores (kcal/mol) for sunitinib and the newly synthesized compounds against the VEGFR2, associated with PDB ID: 2OH4. The recorded RMSD value is 1.9072

No	Name	Docking score
1	Sunitinib	-7.086
2	MI8	-7.403
3	MI7	-6.429
4	MI6	-6.413
5	MI9	-6.247

Table 2: The docking scores (kcal/mol) for doxorubicin and the newly synthesized compounds against the topoisomerase II, associated with PDB ID: 5GWK. The recorded RMSD value is 0.2394.

No	Name	Docking score
1	doxorubicin	-4.761
2	MI8	-5.194
3	MI6	-4.887
4	MI9	-4.843
5	MI7	-4.609

In respect to compound MI8, which docked with topoisomerase II, exhibited a docking score of (-5.194) kcal/mol, higher than that of doxorubicin. The binding of this compound involved a hydrogen bond between H1E11 and the nitrogen of the thiadiazol ring and a hydrogen bond between GLY150, GLY149, and TYR155 and the ketone group of anthraquinone, and Pi-pi stacking of PHE106 with the benzene ring of anthraquinone (Fig.3).

Chemistry

Scheme 1 demonstrates the synthetic strategies utilized to obtain the final target compounds MI6, MI7, MI8, and MI9. This technique uses anhydrous sodium carbonate and carbon disulfide to convert thiosemicarbazide into 2-amino-5-mercapto-1,3,4-thiadiazole; ethanol is the solvent.

Ameen and Qasir [2012] afterward, we synthesize the corresponding compounds by S-alkylation on compound 1 using triethylamine as a base, along with various benzyl chlorides. 2f-2i

Al-Hashemmi and Muthanna (2024) thionyl chloride serves as the coupling agent to facilitate amide bond formation, where amines (compounds 2f-2i) are reacted with anthraquinone-carboxylic acid. This process yields a diverse range of derivatives of anthraquinone (Jabber, 2022).

With respect to the formation of intermediate 1, it involved the reaction of thiosemicarbazide with sodium carbonate. The base (Na₂CO₃) deprotonates the amide nitrogen, generating an enolate ion. This step involves a shift in the electron density, which results in a resonance structure where the negative charge is localized on the sulfur atom.

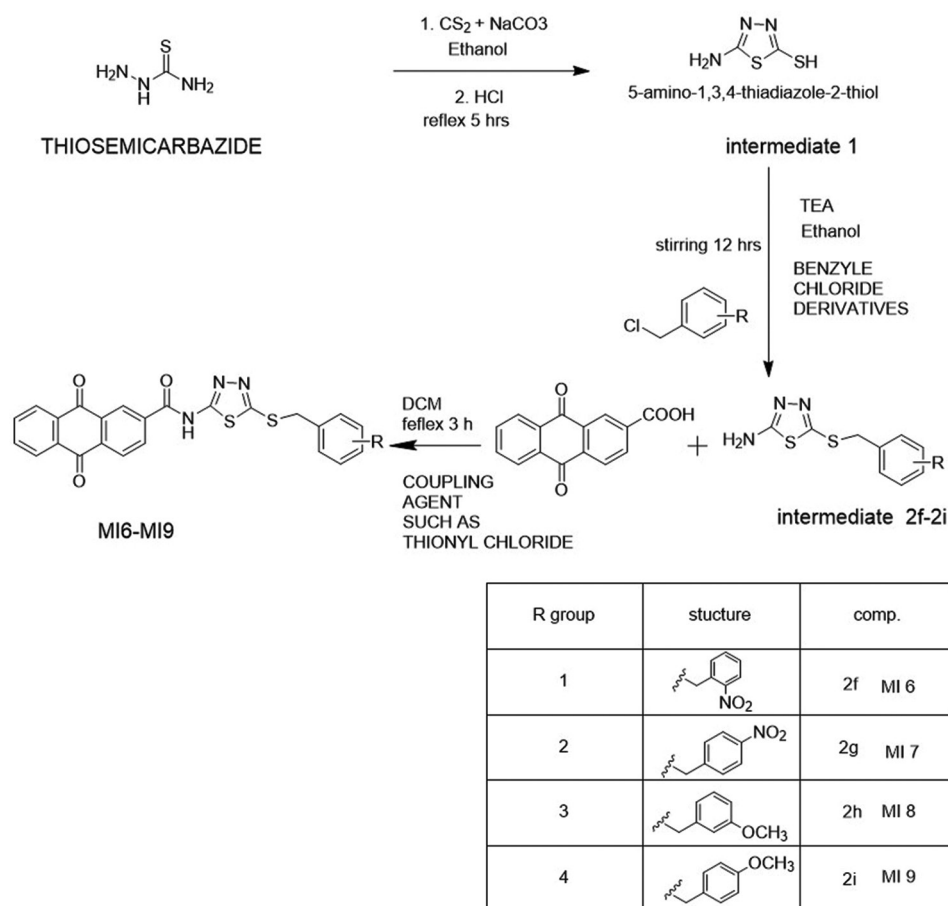
The enolate ion then reacts with carbon disulfide (CS₂), which leads to the formation of a thioamide intermediate where the carbon of the CS₂ is bonded to the sulfur in the thiosemicarbazide.

The next part of the reaction shows thion-thiol tautomerism, which refers to the interconversion between two structural forms: a thion form (where the sulfur atom is doubly bonded to carbon) and a thiol form (where the sulfur atom is bonded to hydrogen and carbon). In this case, 5-amino-1,3,4-thiadiazole-2-thione (the thion form) can shift to 5-amino-1,3,4-thiadiazole-2-thiol (the thiol form), and this interconversion is promoted by the environment, such as an acid (HCl) or base. The tautomerism involves the exchange of a hydrogen atom and a sulfur atom, leading to different bonding patterns.

The S-alkylation reaction, the suggested mechanism for the synthesis of compounds 2f-2i in an alkaline environment, is as follows: the TEA deprotonates the intermediate 1 to produce thiolate anion, which attacks the adjacent carbon (benzylic Carbon) bonded to the chlorine atom; the halogen functions as an electron-withdrawing, leaving group, facilitating the reaction.

The final step involved a nucleophilic acyl substitution mechanism, wherein the carboxylic acid is converted into a chlorosulfite intermediate, with the hydroxyl group of the acid being substituted by a significantly more favorable leaving group. Anthraquinone 2-carboxylic acid chloride is produced when chlorosulfite interacts with a nucleophilic chloride ion. Then the reaction begins with a primary alkylamine (represented by NH₂-R₂) attacking the activated acyl group (R1-C-Cl). The amine acts as a nucleophile, meaning it donates a pair of electrons to form a bond with the carbonyl carbon. The nucleophilic attack leads to the formation of a tetrahedral intermediate. This intermediate is an unstable structure where the nitrogen (NH₂) is attached to the carbonyl carbon, and the chloride (Cl) group is displaced.

The tetrahedral intermediate rearranges, forming activated amino alkyl derivatives. These products are shown to have a specific structure where R1 and R2 are specific substituents attached to the nitrogen and carbon atoms.



Scheme 1: Synthesis of anthraquinone derivative compounds

The reaction progresses with the elimination of X (likely a leaving group, possibly chloride), which is replaced by an alkyl group attached to the nitrogen, resulting in the final products.

Attenuated total reflectance-FTIR spectra

The particular appearance and disappearance of peaks in the given IR spectroscopic analyses defined the synthesized compounds, as shown in Table 3.

The following distinctive bands are displayed in the FT-IR spectrum of intermediate 1. The asymmetric and symmetric stretching vibrations of the -NH₂ group were responsible for the two bands in the 3329 cm⁻¹ and 3248 cm⁻¹, respectively. The -NH stretching (tautomeric form) was responsible for the absorption band at 3109 cm⁻¹. The -NH group was intramolecularly hydrogen bonded, which was responsible for the bands at 2924 cm⁻¹ and 2762 cm⁻¹. At 2600 cm⁻¹, the SH stretching band revealed a very weak shoulder. The thiadiazol ring moiety's (C=N) stretching caused a band at 1604 cm⁻¹. The (N-H) bending and (C-N) stretching vibrations are responsible for the sharp bands at 1550 cm⁻¹ and 1469 cm⁻¹, respectively. In addition, the (C=S) group's absorption band at 1361 cm⁻¹ shows that compound [1] can exist in two tautomeric forms: thiol and thion form. In addition, the (C-S) bond-induced band at 675 cm⁻¹ provides strong support for the product's structure.

In respect to Compounds 2f-2i are characterized by two distinct absorption bands in the range of 3300–3250 cm⁻¹, indicating the

presence of a primary amine. Moreover, a band of aromatic CH around 3010, and the presence of a band of aliphatic CH around 2950 cm⁻¹.

Finally, the final compounds MI6–MI9 are characterized by the disappearance of the two bands of primary amine and are replaced by a single band of secondary amine between 3160 cm⁻¹ and 3190 cm⁻¹. In addition, the absence of the carbonyl group band of the carboxylic acid at 1693 cm⁻¹ is observed, replaced by a distinct and sharp band corresponding to the amide carbonyl group appearing around 1655 cm⁻¹.

The ¹H-NMR spectra

The ¹H-NMR spectra supported the proposed derivative structure (Table 4).

- The compound MI6 was characterized by the presence of an amide proton singlet at 12.22 and a characteristic peak at chemical shift 4.63 ppm (singlet), which is for two hydrogens at benzylic carbon and other peaks in the aromatic region (7.53–8.54 ppm) m, 11H, aromatic protons.
- The compound MI7 was characterized by the presence of an amide proton singlet at 12.28 and a characteristic peak at chemical shift 4.54 ppm (singlet), which is for two hydrogens at benzylic carbon and other peaks in the aromatic region (7.54–8.55 ppm) m, 11H, aromatic protons.
- The compound MI8 was characterized by the presence of a characteristic peak at chemical shift 3.74 ppm (singlet), which is for three hydrogens of the methoxy group and an amide proton

Table 3: The ATR-FTIR spectra of both the final compounds and their intermediates

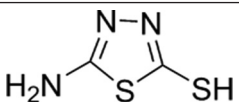
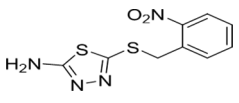
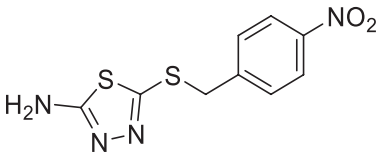
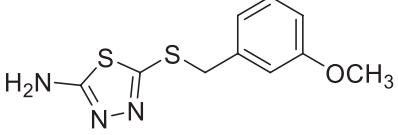
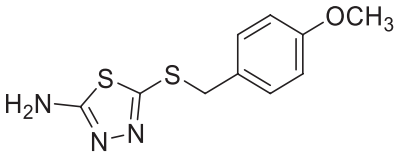
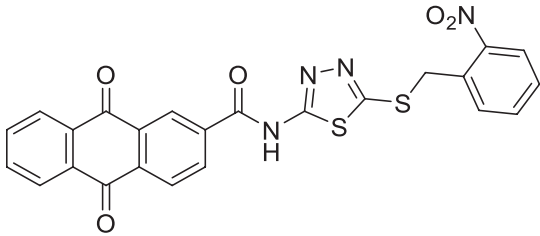
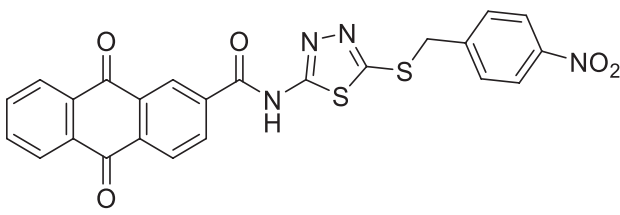
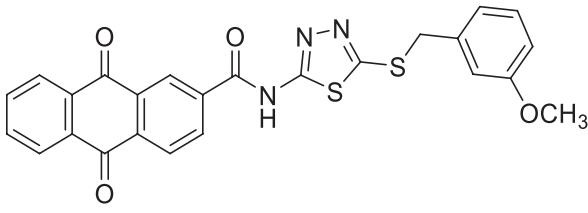
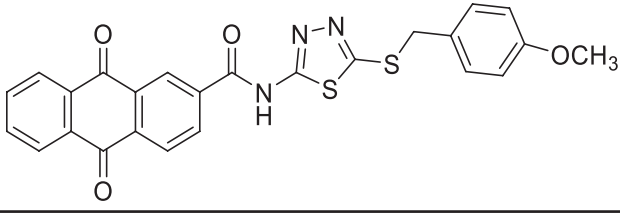
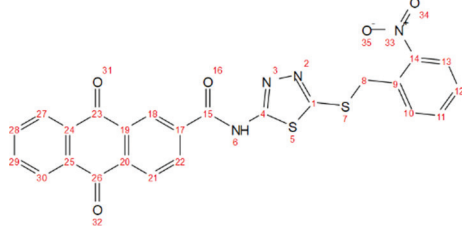
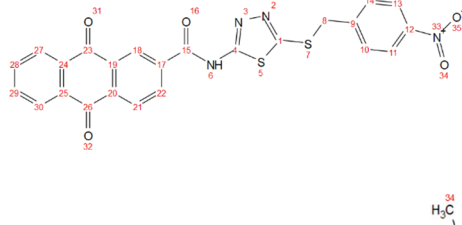
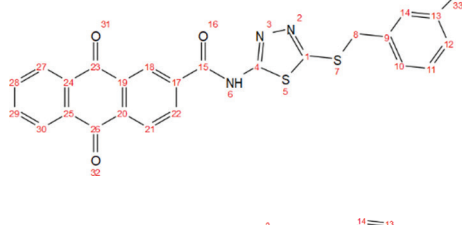
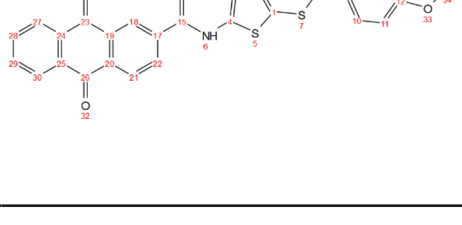
Interpretation	Chemical structure	Compound
3329,3248 (NH2) stretching of primary amine 1604 (C=N) stretching of the imine bond. 1361 (C=S) stretching.		1
3278 (NH) stretching of primary amine, 3074 (C-H) stretching of the aromatic ring, 2951 aliphatic (C-H) stretching 1635 (C=N) stretching of the imine bond 1608,1504(C=C) stretching of the aromatic ring		2f
3275 (NH) stretching of primary amine 3093 (C-H) stretching of the aromatic ring 2954 aliphatic (C-H) stretching, 1631 (C=N) stretching of the imine bond 1600,1523 (C=C) stretching of the aromatic ring		2g
3305,3259(NH) stretching of primary amine 3082 (C-H) stretching of the aromatic ring 2966 aliphatic (C-H) stretching 1631 (C=N) stretching of the imine bond 1585,1492 (C=C) stretching of the aromatic ring.		2h
3315 (NH) stretching of primary amine 3088 (C-H) stretching of the aromatic ring 2931 aliphatic (C-H) stretching 1629 (C=N) stretching of the imine bond, 1608,1512 (C=C) stretching of the aromatic ring.		2i
3170 (NH) stretching of secondary amine 3039(C-H) stretching of the aromatic ring 2953 aliphatic (C-H) stretching 1676 (C=O) of ketone 1646 (C=O) of amide 1537,1452 (C=C) stretching of the aromatic ring. 1556, 1346 (N-O) stretching		MI6
3165 (NH) stretching of secondary amine 3066 (C-H) stretching of the aromatic ring 2958 aliphatic (C-H) stretching 1673 (C=O) of ketone 1654 (C=O) of amide 1587,1487 (C=C) stretching of the aromatic ring. 1514,1344 (N-O) stretching		MI7
3175 (NH) stretching of secondary amine 3037(C-H) stretching of the aromatic ring 2950 aliphatic (C-H) stretching 1674 (C=O) of ketone 1652 (C=O) of amide 1586,1454 (C=C) stretching of the aromatic ring. 1043 aromatic (C-O) stretching		MI8
3163 (NH) stretching of secondary amine 3058 (C-H) stretching of the aromatic ring 2924 aliphatic (C-H) stretching 1676 (C=O) of ketone 1653 (C=O) of amide 1589,1539 (C=C) stretching of the aromatic ring. 1097 aromatic (C-O) stretching.		MI9

Table 4: The ¹H-NMR spectra for the final compounds

Assignment (atom number)	Chemical shift (δ), (splitting, integration)	Structure	Comp.
8	4.63(s, 2 H)		MI6
12	7.53 (t, 1H)		
11	7.65 (t, 1H)		
10	7.7 (d, 1H)		
13	8.03 (d, 1H)		
28,29	7.85 (t, 2H)		
27,3	8.11 (d, 2H)		
21,22	8.26 (d, 2H)		
18	8.54 (s, 1H)		
6	12.22 (s, 1H)		
8	4.54(s, 2 H)		MI7
10,14	7.62 (d, 2H)		
11,13	8.15 (d, 2H)		
28,29	7.81 (t, 2H)		
27,3	8.10 (d, 2H)		
21,22	8.25 (d, 2H)		
18	8.55 (s, 1H)		
6	12.28 (s, 1H)		
34	3.74 (s, 3H)		
8	4.69(s, 2 H)		
12	6.83 (d, 1H)		MI8
14	6.86 (s, 1H)		
10	7.14 (d, 1H)		
11	7.25 (t, 1H)		
28,29	7.83 (t, 2H)		
27,3	8.11 (d, 2H)		
21,22	8.24 (d, 2H)		
18	8.58 (s, 1H)		
6	12.13 (s, 1H)		
34	3.63 (s, 3H)		
8	4.27(s, 2 H)		MI9
11,13	6.86 (d, 2H)		
10,14	7.13 (d, 2H)		
28,29	7.84 (t, 2H)		
27,3	8.13 (d, 2H)		
21,22	8.24 (d, 2H)		
18	8.56 (s, 1H)		
6	12.38 (s, 1H)		

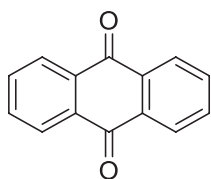


Fig. 1: Anthraquinone

singlet at 12.13 and a characteristic peak at chemical shift 4.69 ppm (singlet) which is for two hydrogens at benzylic carbon and other peaks in the aromatic region (6.83–8.58 ppm) m, 11 H, aromatic protons.

- The compound MI9 was characterized by the presence of a characteristic peak at chemical shift 3.63 ppm (singlet), which is for three hydrogens of the methoxy group and an amide proton singlet at 12.38 and a characteristic peak at chemical shift 4.27 ppm (singlet) which is for two hydrogens at benzylic carbon and other peaks in the aromatic region (6.86–8.56 ppm) m, 11 H, aromatic protons.

MTT assay

Compound MI8 exhibits the strongest inhibitory effect on breast cancer (MDA-MB-231) cell growth in preliminary results from the MTT assay compared to sunitinib and doxorubicin. Similarly,

Table 5: The IC₅₀ value, measured in μM, for the breast cancer

No.	Name	IC ₅₀ μM	±SD
1	Doxorubicin	5.32	±0.05
2	Sunitinib	17.27	±0.09
3	MI8	6.15	±2.48
4	MI6	92.55	±5.31
5	MI7	52.56	±0.13
6	MI9	111.91	±1.45

Table 6: The IC₅₀ value, measured in μM, for the lung cancer

No.	Name	IC ₅₀ μM	±SD
1	Doxorubicin	5.21	±0.03
2	Sunitinib	7.52	±0.04
3	MI8	8.41	±0.54
4	MI9	9.25	±0.16
5	MI6	127.58	±5.21
6	MI7	130.46	±4.78

findings from the lung cancer (A549) cell growth assay reveal that compounds MI8 and MI9 achieve the most significant inhibition, outperforming both doxorubicin and sunitinib, as detailed in Tables 5 and 6.

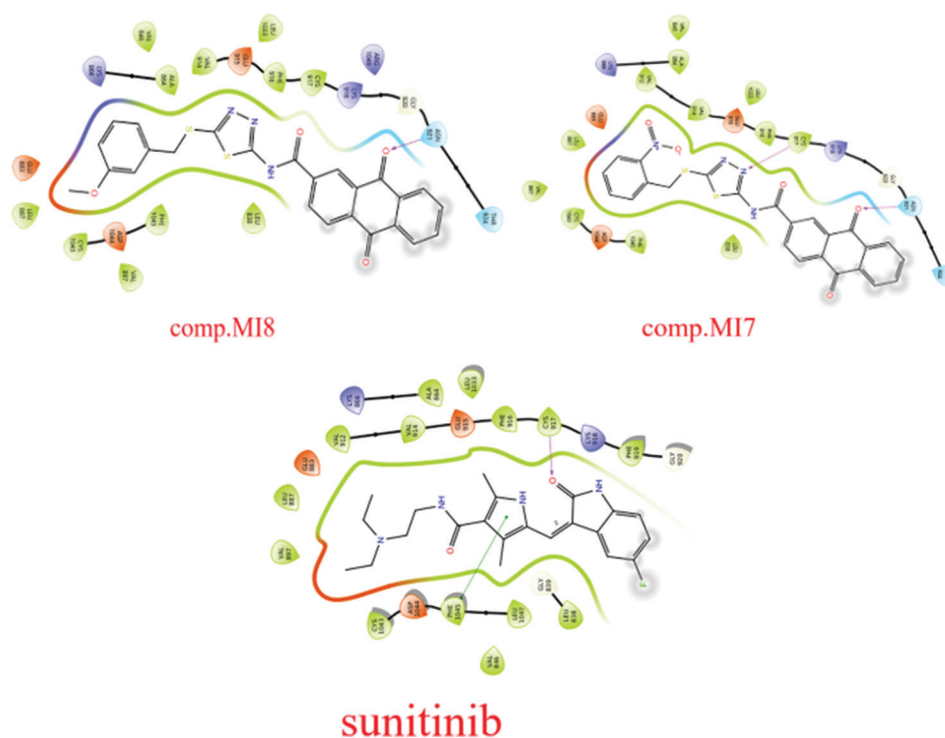


Fig. 2: The interaction of MI1 and MI2, along with sunitinib, with Vegfr2 is analyzed within a two-dimensional framework

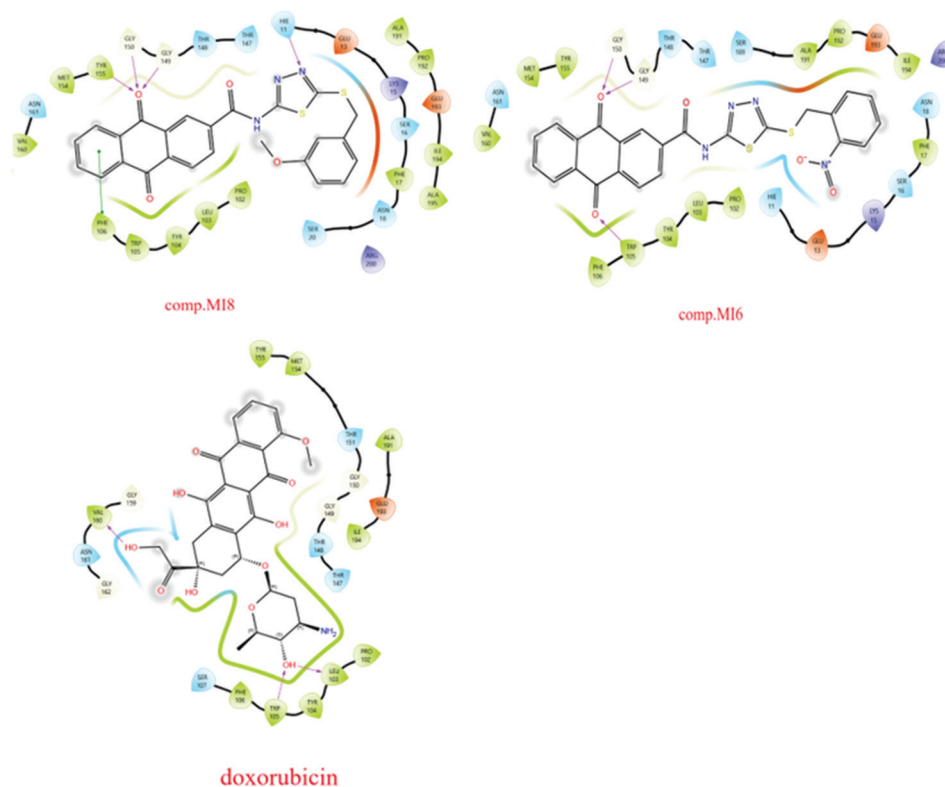


Fig. 3: Illustrates the two-dimensional interplay among doxorubicin, MI1, and MI5in relation to their interaction with topoisomerase II

CONCLUSION

The synthesized molecules, designated as MI6-MI9, were successfully developed, and their chemical structures were extensively characterized using proton nuclear magnetic resonance ($^1\text{H-NMR}$) spectroscopy and FT-IR spectroscopy. In comparison to sunitinib and doxorubicin, MI8

and MI9 demonstrated superior cell inhibition activity, demonstrating a strong potential for inhibiting cell proliferation. The molecular modeling analyses and biological evaluations showed a remarkable consistency with the anticipated outcomes. These findings are extremely promising and could significantly contribute to advancing the design of novel antiproliferative compounds. The current finding

concerning compound MI8 is highly promising, and further molecular dynamic simulation, *in vivo* studies, and structure–activity relationships are able to verify the existing data.

ACKNOWLEDGMENTS

The authors extend their gratitude to the Pharmacy College at Baghdad University for providing their valuable support.

CONFLICT OF INTEREST

The author stated that there are no conflicts of interest to disclose.

ETHICS STATEMENTS

As authors, we certify that our signing of this form guarantees that the presented work complies with ethical standards; no human or animal samples were used in this work.

AUTHORS' CONTRIBUTIONS

Mohammed Hassan Mohammed played a key role in the design and molecular modeling process by participating in the synthesis and testing of the compounds, as well as organizing and drafting the manuscript. Mohammed Ismail Mohammed was tasked with designing, synthesizing, purifying, and evaluating the cytotoxic activity of the final molecules, in addition to contributing to the manuscript's preparation.

REFERENCES

1. Abbas AH. Synthesis, Docking Study, and Cytotoxic Evaluation of New 2-Pyridine Derivatives. Baghdad: University of Baghdad; 2021.
2. Abouzied AS, Al-Humaidi JY, Bazaid AS, Qanash H, Binsaleh NK, Alamri A, *et al.* Synthesis, molecular docking study, and cytotoxicity evaluation of some novel 1,3,4-thiadiazole as well as 1,3-thiazole derivatives bearing a pyridine moiety. *Molecules*. 2022;27(19):6368. doi: 10.3390/molecules27196368, PMID 36234908
3. Al-Hashemmi A, Muthanna SF. Synthesis, identification, and preliminary pharmacological evaluation of new hydrazone and 1,3,4-oxadiazole derivatives of ketorolac. *Iraqi J Pharm Sci*. 2024;33(1):113-22. doi: 10.31351/vol33iss1pp113-122
4. Ali A, Smith J. Cancer is a group of diseases characterized by the uncontrolled growth and spread of abnormal cells in the body. *Cancer Research*. 2020;80(5):1023-1031. doi:10.1158/0008-5472.CAN-19-1234.
5. Ali AA, Lee YR, Chen TC, Chen CL, Lee CC, Shiau CY, *et al.* Novel anthra[1,2-c][1,2,5]thiadiazole-6,11-diones as promising anticancer lead compounds: Biological evaluation, characterization & molecular targets determination. *PLoS One*. 2016;11(4):e0154278. doi: 10.1371/journal.pone.0154278, PMID 27100886
6. Ali RM, Al-Hamashi A. Design, synthesis, and preliminary antiproliferative evaluation of 1,2,4-thiadiazole derivatives as possible histone deacetylase inhibitors. *Iraqi J Pharm Sci*. 2024;33(4SI):57-66.
7. Ameen HA, Qasir AJ. Synthesis and preliminary antimicrobial study of 2-amino-5-mercapto-1,3,4-thiadiazole derivatives. *Iraqi J Pharm Sci*. 2012;21(1):98-104.
8. Andreeva DV, Vedekhina TS, Gostev AS, Dezhnekova LG, Volodina YL, Markova AA, *et al.* Thiadiazole-, selenadiazole-, and triazole-fused anthraquinones as G-quadruplex targeting anticancer compounds. *Eur J Med Chem*. 2024;268:116222. doi: 10.1016/j.ejmech.2024.116222, PMID 38387333
9. Bray F, Ferlay J, Soerjomataram I, Siegel RL, Torre LA, Jemal A. Global cancer statistics 2018: GLOBOCAN estimates of incidence and mortality worldwide for 36 cancers in 185 countries. *CA Cancer J Clin*. 2018;68(6):394-424. doi: 10.3322/caac.21492, PMID 30207593
10. Global Burden of Disease Cancer Collaboration, Fitzmaurice C, Dicker D, Pain A, Hamavid H, Moradi-Lakeh M, *et al.* The global burden of cancer 2013. *JAMA Oncol*. 2015;1(4):505-27. doi: 10.1001/jamaoncol.2015.0735, PMID 26181261
11. ICGC/TCGA Pan-Cancer Analysis of Whole Genomes Consortium. Pan-cancer analysis of whole genomes. *Nature*. 2020;578(7793):82-93. doi: 10.1038/s41586-020-1969-6, PMID 32025007
12. Dakhel Z, Mohammed M. Synthesis of new sulfonamide derivatives-phenylalanine and proline ester conjugate using maleimide spacer as anticancer agents. *Int J Pharm Sci Rev Res*. 2018;43:169-77.
13. Drapak IV, Zimenkovsky BS, Slaby MV, Holota SM, Perekhoda LO, Yaremkevych RV, *et al.* Synthesis and diuretic activity of novel 5-amino-1,3,4-thiadiazole-2-thiol derivatives. *Biopolym Cell*. 2021;37(1):33-45. doi: 10.7124/bc.000A4A
14. Fan J, Fu A, Zhang L. Progress in molecular docking. *Quant Biol*. 2019;7(2):83-9. doi: 10.1007/s40484-019-0172-y
15. Hasan SM, Samir AH. Synthesis and characterization of novel Schiff bases of imide moiety. *Ibn Al-Haitham J Pure Appl Sci*. 2017;27(3):407-20.
16. Jabber MM, Hadi MK. Synthesis, characterization, and antimicrobial evaluation of new ibuprofen derivatives. *Pak J Med Health Sci*. 2022;16(3):689. doi: 10.53350/pjmhs22163689
17. Janowska S, Khylyuk D, Bielawska A, Szymanowska A, Gornowicz A, Bielawski K, *et al.* New 1,3,4-thiadiazole derivatives with anticancer activity. *Molecules*. 2022;27(6):1814. doi: 10.3390/molecules27061814, PMID 3535177
18. Janowska S, Paneth A, Wujec M. Cytotoxic properties of 1,3,4-thiadiazole derivatives-a review. *Molecules*. 2020;25(18):4309. doi: 10.3390/molecules25184309, PMID 32962192
19. Khalil NA, Kamal AM, Emam SH. Design, synthesis, and antitumor activity of novel 5-pyridyl-1,3,4-oxadiazole derivatives against the breast cancer cell line MCF-7. *Biol Pharm Bull*. 2015;38(5):763-73. doi: 10.1248/bpb.b14-00867, PMID 25947922
20. Leiter A, Veluswamy RR, Wisnivesky JP. The global burden of lung cancer: Current status and future trends. *Nat Rev Clin Oncol*. 2023;20(9):624-39. doi: 10.1038/s41571-023-00798-3, PMID 37479810
21. Li Y, Jiang JG. Health functions and structure-activity relationships of natural anthraquinones from plants. *Food Funct*. 2018;9(12):6063-80. doi: 10.1039/c8fo01569d, PMID 30484455
22. Mahdi GA, Dakhel ZA. Synthesis, characterization, and preliminary pharmacological evaluation of new naproxen containing 1,3,4-thiadiazole-2-thiol derivatives. *Iraqi J Pharm Sci*. 2024;33(4SI):349-61.
23. Malik MS, Alsantali RI, Jassas RS, Alsimaree AA, Syed R, Alsharif MA, *et al.* Journey of anthraquinones as anticancer agents-a systematic review of recent literature. *RSC Adv*. 2021;11(57):35806-27. doi: 10.1039/d1ra05686g, PMID 35492773
24. Mishra B, Acharya PC, De UC. Redefining anthraquinone-based anticancer drug design through subtle chemical modifications. *Anticancer Agents Med Chem*. 2025;25(16):1161-74. doi: 10.2174/0118715206374787250227064528, PMID 40033586
25. Mohammed ZM, Al-Hamashi AA. Molecular docking, molecular dynamic simulation, ADMET, synthesis, and preliminary cytotoxic activity of new triazole-based derivatives with expected histone deacetylase inhibition activity. *Iraqi J Pharm Sci*. 2024;33(4SI):101-10.
26. Ogurtsov AY, Mariño-Ramírez L, Johnson GR, Landsman D, Shabalina SA, Spiridonov NA. Expression patterns of protein kinases correlate with gene architecture and evolutionary rates. *PLoS One*. 2008;3(10):e3599. doi: 10.1371/journal.pone.0003599, PMID 18974838
27. Pham EC, Truong TN, Dong NH, Vo DD, Hong Do TT. Synthesis of a series of novel 2-amino-5-substituted 1,3,4-oxadiazole and 1,3,4-thiadiazole derivatives as potential anticancer, antifungal, and antibacterial agents. *Med Chem*. 2022;18(5):558-73. doi: 10.2174/1573406417666210803170637, PMID 34344293
28. Roskoski R. A historical overview of protein kinases and their targeted small molecule inhibitors. *Pharmacol Res*. 2015;100:1-23. doi: 10.1016/j.phrs.2015.07.010, PMID 26207888
29. Sabit H, Abdel-Hakeem M, Shoala T, Abdel-Ghany S, Abdel-Latif MM, Almulhim J, *et al.* Nanocarriers: A reliable tool for the delivery of anticancer drugs. *Pharmaceutics*. 2022;14(8):1566. doi: 10.3390/pharmaceutics14081566, PMID 36015192
30. Sahib H, Dakhel Z, Hadi M. Synthesis and preliminary antimicrobial activity evaluation of new amide derivatives of 2-aminobenzothiazole. *Int J Drug Deliv Technol*. 2021;11:1258-61. doi: 10.25258/ijddt.11.4.23
31. Abduljabbar T, Hadi MK. Synthesis, characterization, and antibacterial evaluation of some coumarin derivatives. *Iraqi J Pharm Sci*. 2021;30(1):249-57. doi: 10.31351/vol30iss1pp249-257
32. Thandra KC, Barsouk A, Saginala K, Aluru JS, Barsouk A. Epidemiology of lung cancer. *Contemp Oncol (Pozn)*. 2021;25(1):45-52. doi: 10.5114/wo.2021.103829, PMID 33911981
33. Tian W, Wang C, Li D, Hou H. Novel anthraquinone compounds as anticancer agents and their potential mechanism. *Fut Med Chem*. 2020;12(7):627-44. doi: 10.4155/fmc-2019-0322, PMID 32175770
34. Wassel MM, Ammar YA, Elhag Ali GA, Belal A, Mehany AB, Ragab A. Development of adamantane scaffold containing 1,3,4-thiadiazole derivatives: Design, synthesis, anti-proliferative activity, and molecular docking study targeting EGFR. *Bioorg Chem*. 2021;110:104794. doi: 10.1016/j.bioorg.2021.104794, PMID 33735711
35. Wu S, Zhou X, Li F, Sun W, Zheng Q, Liang D. Novel anthraquinone-based benzenesulfonamide derivatives and their analogues as potent human carbonic anhydrase inhibitors with antitumor activity: Synthesis, biological evaluation, and *in silico* analysis. *Int J Mol Sci*. 2024;25(6):3348. doi: 10.3390/ijms25063348, PMID 38542320